PCCP

Interplay Between Hydrogen Atmosphere and Dislocation Characteristics (Core and Elastic Energies, Interaction Energy, and Character Angle) in BCC Fe from Time-Averaged Molecular Dynamics

SCHOLARONE™
Manuscripts

Interplay Between Hydrogen Atmosphere and Dislocation Characteristics in BCC Fe from Time-Averaged Molecular Dynamics

C. Nowak[1], and X. W. Zhou[1]

[1]*Sandia National Laboratories, Livermore, California 94550, USA*

Abstract

The interplay between hydrogen and dislocations (e.g., core and elastic energies, dislocation-dislocation interactions) has implications on hydrogen embrittlement but is poorly understood. Continuum models of hydrogen enhanced local plasticity have not considered the effect of hydrogen on dislocation core energies. Energy minimization atomistic simulations can only resolve dislocation core energies in hydrogen-free systems because hydrogen motion is omitted so hydrogen atmosphere formation can't occur. Additionally, previous studies focused more on face-centered-cubic than body-centered-cubic metals. Discrete dislocation dynamics studies of hydrogen - dislocation interactions assume isotropic elasticity, but the validity of this assumption isn't understood. We perform time-averaged molecular dynamics simulations to study the effect of hydrogen on dislocation energies in body-centered-cubic iron for several dislocation character angles. We see atmosphere formation and highly converged dislocation energies. We find that hydrogen reduces dislocation core energies but can increase or decrease elastic energies of isolated dislocations and dislocation - dislocation interaction energies depending on character angle. We also find that isotropic elasticity can be well fit to dislocation energies obtained from simulations if the isotropic elastic constants are not constrained to their anisotropic counterparts. These results are relevant to ongoing efforts in understanding hydrogen embrittlement and provide a foundation for future work in this field.

Keywords: Hydrogen embrittlement, hydrogen - dislocation interactions, molecular dynamics, dislocation energies, hydrogen atmosphere, body-centered-cubic iron, dislocation character angle

I.   INTRODUCTION

Hydrogen (H) embrittlement imposes a critical challenge for structural materials used in hydrogen energy applications [1,2]. In this regard, hydrogen - dislocation interactions remain to be one of the focal research areas on hydrogen embrittlement because dislocation migration is the vehicle for plastic deformation and the dislocation strain field can significantly elevate hydrogen concentration at dislocation core [3]. Traditionally, hydrogen embrittlement has been related to the hydrogen-enhanced local plasticity (HELP) mechanism [4-6]. As one HELP effect, hydrogen can "screen" interactions between dislocations, and therefore reduces dislocation spacing in dislocation pileups to promote coalescence at crack tips leading to fracture [7]. As another HELP effect, hydrogen increases mobility of local dislocations [8-10], and therefore cause strain concentration also leading to fracture. Hydrogen - dislocation interactions can be quantified by hydrogen effects on dislocation energies. Despite extensive studies using both continuum models [11] and atomistic approaches such as molecular statics [12], Monte Carlo [10], and first-principles [13] calculations, our current understanding of hydrogen effects on dislocation energies remains poor. The primary knowledge gaps include: (1) continuum models have not considered the hydrogen effects on dislocation core energies; (2) previous atomistic simulations mostly treat hydrogen as frozen atoms whereas hydrogen atoms in experiments always exhibits a "cloud" nature due to their high mobilities; (3) past studies of dislocation energies are mostly focused on face-centered-cubic (FCC) materials [14,15] and behavior in body-centered-cubic (BCC) materials

is relatively less explored [16,17]; and (4) while discrete dislocation dynamics (DDD) [18-20] is effective to reveal dislocation behavior on a mesoscale, dislocation energies in DDD simulations are typically constructed from isotropic elasticity theory and the impact of this approximation has never been explicitly explored.

The objectives of this work are threefold: (1) extend the time-averaged molecular dynamics (MD) method [21,22] to include hydrogen effects where the cloud nature of hydrogen can be accurately captured; (2) calculate dislocation energies under a variety system dimensions and dislocation character angles for an elastically anisotropic α-Fe to quantify the approximation of isotropic theories in DDD simulations; (3) study effects of hydrogen on dislocation core energies, dislocation elastic energies, and dislocation interaction energies in the entire range of dislocation character angles ($-90^{\circ} - 90^{\circ}$); and (4) discuss our results in the context of hydrogen embrittlement. The α-Fe is chosen for study as it is the basis for the low-cost widely used Fe-C steel, a BCC metal, and has anisotropic elastic constants.

II.   METHODOLOGY

A. Geometries

Dislocation energy can be calculated from energy difference between systems with and without dislocations. Systems without dislocations can be easily created. For systems with dislocations, we study dislocation dipole configurations so that full periodic boundary conditions can be applied in all three directions. In general, our dislocation dipole configurations and sizes are schematically illustrated in Fig. 1, where the x, z, and y directions are aligned with the $\langle 111 \rangle$ burgers vector $\vec{b}$, the dislocation line $\vec{\xi}$, and the $\langle 110 \rangle$ directions respectively. Hence, the x and z axes can be non-orthogonal, but the y axis is always orthogonal to the x-z slip plane. Such a

dislocation dipole can be easily created using the previous approach [22] for any designated character angle β ≠ 0. Under the periodic boundary conditions, Fig. 1 essentially prescribes an infinite array of dislocation dipoles whose horizontal spacing is S, vertical spacing is L_y, and dipole distance is d, with dislocation character angle β ≠ 0.
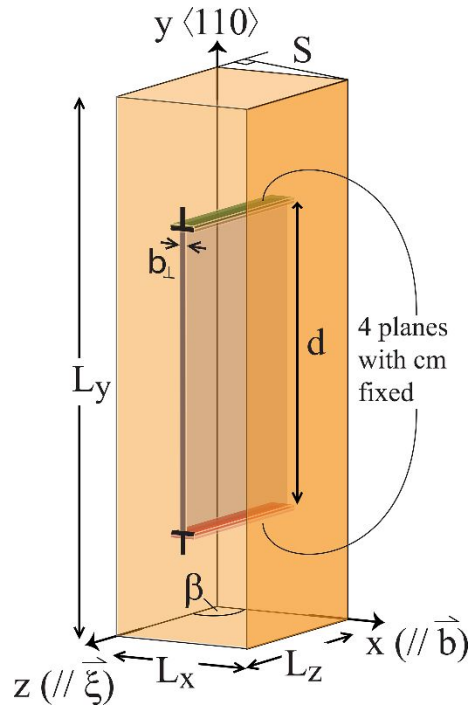

Figure 1. Schematic of the simulation cells used in this work. The x, z, and y directions are aligned with the burgers vector $\vec{b}$, the dislocation line $\vec{\xi}$, and the slip plane normal.

Unlike FCC materials, the dislocation character angle in BCC systems is not symmetric (i.e., ±β are not equivalent) [23]. As such, we study 31 different angles between -90° and 90°: 5.77°, 10.02°, 15.79°, 19.47°, 25.24°, 27.21°, 35.26°, 43.31°, 45.29°, 51.06°, 54.74°, 60.50°, 64.76°, 70.53°, 76.74°, 78.58°, 84.95°, 90.00°, -11.42°, -14.42°, -19.47°, -25.24°, -29.50°, -35.26°, -38.94°, -54.74°, -6.21°, -70.53°, -74.21°, -79.98°, -84.23°. The choice of angles is based on the required simulation cell size to maintain periodic boundaries for a given angle. We also chose our system dimensions such that L_y ~200 Å, L_z ~60 Å, and vary L_x to control the dislocation spacing

S ($S = L_x \sin \beta$). For hydrogen-containing systems, 0.005 (H/Fe ratio) hydrogen atoms are randomly placed at interstitial sites. Our systems are on average ~80,000 atoms, giving an averaged hydrogen loading of ~400 atoms. We find that upon atmosphere formation, the difference in far-field concentrations to only deviate by ~2.5% amongst each other, so we take this as equivalent loading conditions (chemical potential) across all systems.

B. Simulation Details

The Fe-C-H bond-order potential [24] was used to simulate our systems. The elastic parameters of this potential agree with DFT simulations and experiment [25,26]. We use DFT results as the benchmark as our elastic constants as experimental measurements are often for polycrystalline samples. We use LAMMPS [27,28] for all MD simulations at zero pressure and 1000 K temperature. After 1 ns equilibration, time-averaged potential energy is calculated for the next 10 ns. These time-averaged energies are used to calculate dislocation energies. We found dislocations always migrate back-and-forth during MD simulations [29,30]. To compare dislocation energies from MD and continuum calculations, stationary dislocations are required. To ensure stationary dislocations in MD simulations, we fix center of mass (cm) of four local planes immediate above and below dislocations (see Fig. 1). This has been shown to effectively pin the positions of dislocations without impacting dislocation core structures [29].

C. Continuum Expression of Dislocation Line Energy

To calculate the dislocation line energy per unit length, Γ, from simulation data we use:

$$\Gamma = \frac{E_d - E_b\left(N_d/N_b\right)}{2 * L_d} \tag{1}$$

Where E_d and E_b are the average potential energy of the bulk and dislocation dipole containing systems. N_d and N_b are the number of atoms in the bulk and dislocation dipole containing systems.

L_d is the length of dislocation line. The factor of two in the denominator is included because our system is dislocation dipole. MD dislocation energies under periodic boundaries must be fitted to a continuum elastic energy expression to derive dislocation core energies. Based on the isotropic elasticity theory, this continuum dislocation energy is given as [21,22,31-33].

$$\Gamma = \begin{cases} E_c + \frac{Gb^2\sin^2\beta}{4\pi(1-v)}\left[\ln\frac{1}{r_0} + c_{ue0}(d,S) + c_{ue}(d,S)\right] \\ + \frac{Gb^2\cos^2\beta}{4\pi}\left[\ln\frac{1}{r_0} + c_{us0}(d,S) + c_{us}(d,S)\right] \end{cases} \tag{2}$$

where Γ is energy per unit of dislocation line, b is Burgers magnitude, E_c and r_0 are dislocation core energy and core radius, G and v are shear modulus and Poisson's ratio, β is dislocation character angle, and the four functions $c_{ue0}(d,S)$, $c_{ue}(d,S)$, $c_{us0}(d,S)$, $c_{us}(d,S)$ are expressed as:

$$c_{ue0}(d,S) = \ln\left[\frac{(L_y-d)d}{L_y}\right] - \ln\left[Ga\left(\frac{L_y+d}{L_y}\right)\right] - \ln\left[Ga\left(2 - \frac{d}{L_y}\right)\right] \tag{3}$$

$$c_{us0}(d,S) = \ln\left[\frac{(L_y-d)d}{L_y}\right] - \ln\left[Ga\left(\frac{L_y+d}{L_y}\right)\right] - \ln\left[Ga\left(2 - \frac{d}{L_y}\right)\right] \tag{4}$$

$$c_{ue}(d,S) = \sum_{i=1}^{\infty}\left\{\frac{4\pi iS\coth\left(\frac{\pi iS}{L_y}\right)\sin^2\left(\frac{\pi d}{L_y}\right)}{L_y\cosh\left(\frac{2\pi iS}{L_y}\right) - L_y\cos\left(\frac{2\pi d}{L_y}\right)} + \ln\left[\cos^2\left(\frac{\pi d}{L_y}\right) + \coth^2\left(\frac{\pi iS}{L_y}\right)\sin^2\left(\frac{\pi d}{L_y}\right)\right]\right\} \tag{5}$$

$$c_{us}(d,S) = \sum_{i=1}^{\infty}\ln\left[\cos^2\left(\frac{\pi d}{L_y}\right) + \coth^2\left(\frac{\pi iS}{L_y}\right)\sin^2\left(\frac{\pi d}{L_y}\right)\right] \tag{6}$$

where Ga is the Gamma function, and L_y, S, and d are dislocation vertical spacing, horizontal spacing, and dipole distance respectively. Note that when $L_y \rightarrow \infty$ and $S \rightarrow \infty$ with $d = L_y/2$, the dislocation array shown in Fig. 1 becomes isolated dislocation with infinite elastic energy as defined by Eq. (2). When L_y is finite and $S \rightarrow \infty$ with $d = L_y/2$, Eqs. (2) – (6) reduce to:

$$\Gamma_{S=\infty} = E_c + \left[\frac{Gb^2\sin^2\beta}{4\pi(1-v)} + \frac{Gb^2\cos^2\beta}{4\pi}\right]ln\left(\frac{L_y}{\pi r_0}\right) \tag{7}$$

Eq. (7) defines a finite energy because when d is finite, the ± elastic stresses of the opposite dislocations in the dipole cancel in the far field. Eq. (7) provides a good reference for comparing dislocation interactions.

III.   RESULTS

A.   Method Validation

To validate that the effects of hydrogen cloud have been captured, we must demonstrate that time-averaged MD simulations can produce highly converged dislocation energies in the presence of hydrogen. As an example, Figs. 2(a) and 2(b) show dislocation energies ($\beta = 64.76^{\circ}$) as a function of d at fixed $L_y \sim 196$ Å and S ~ 80 Å, and as a function of S at a fixed $d = L_y/2 \sim 98$ Å. Results without (red) and with 0.005 hydrogen (blue) are shown as circles for MD values, and lines are for the continuum fit to be described below.
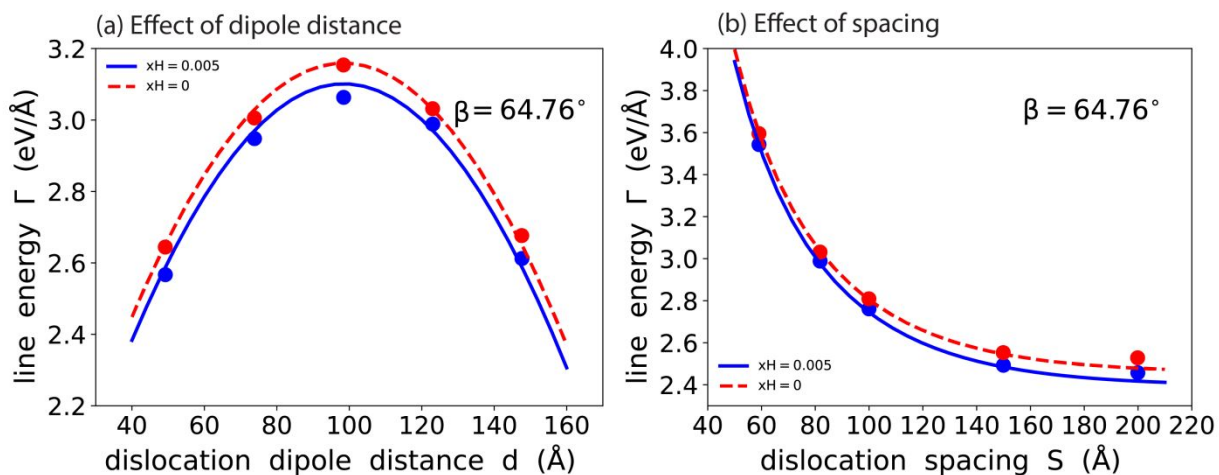

Figure 2. Example results for dislocation energies as a function of (a) dipole distance d and (b) horizontal dislocation spacing S for dislocations with a character angle of $\beta = 64.76^{\circ}$.

Fig. 2 indicates that without hydrogen, the MD results of dislocation energies fall almost exactly on the continuum lines, further confirming the previous results [21,22,33] that the time-averaged approach is effective for calculating dislocation energies without hydrogen. More interestingly, Fig. 2 confirms that even with hydrogen, the MD results of dislocation energies still fall very well on the continuum lines. This validates that the time-averaged MD method not only enables hydrogen to be simulated as an atmosphere around dislocations, but also enables the statistical effect of the atmosphere to converge to a single dislocation energy value. Hence, our method is applicable to studying hydrogen - dislocation interactions.

B. Dislocation Core Energies and Justification of Isotropic Elasticity Theory

Our molecular statics simulations indicated that for the potential we used, the hydrogen-free α-Fe has elastic constants of $C_{11} = 218.033$ GPa, $C_{12} = 141.941$ GPa, and $C_{44} = 129.828$ GPa, giving an anisotropic ratio of $A = 2C_{44}/(C_{11}-C_{12}) = 3.412$. At a first sight, it appears that the isotropic theory, Eqs. (1) – (5), may not be suitable to describe this anisotropic system. However, the only criterion for the applicability of Eqs. (1) – (5) is if they can be well fitted to the MD dislocation energy data obtained from a variety of dislocation spacings. This appears likely since the elastic constants used in Eqs. (1) – (5) do not have to be bounded by C_{11}, C_{12}, and C_{44}, and Eqs. (1) – (5) additionally involve other fitting parameters such as dislocation core energies E_c. To employ our results in larger scale DDD simulations, the results from isotropic theory are required as DDD is built on isotropic theory. We fitted Eqs. (1) – (5) to all our MD results of dislocation energies at a chosen dislocation core radius of $r_c = 2.5$ Å where dislocation core energies are allowed to vary at different character angles but a single set of elastic constants G and ν are obtained for systems with and without hydrogen respectively. Note that an arbitrarily chosen dislocation core radius does not impact results as it is correspondingly corrected by the core

energies [21,22,33]. We found that $G = 0.774$ eV/Å^3 and $\nu = 0.413$ for hydrogen-free systems, and $G = 0.749$ eV/Å^3 and $\nu = 0.434$ for systems containing 0.005 hydrogen. Hence, hydrogen was found to reduce shear modulus.

The fitted dislocation core energies as a function of dislocation character angles are shown in Fig. 3. The dislocation core energies in the $\pm$ angle ranges are not strictly symmetric (assuming that numerical errors are too small to bias the observation), in agreement with the previous work [23]. Interestingly, hydrogen reduces core energies, which is consistent with the notion that hydrogen segregation at dislocation cores is driven by energy minimization. More interestingly, the difference in core energies with and without 0.005 hydrogen seems to follow a cos^2 function, in agreement with previous continuum models [20]. This means that hydrogen reduces more significantly edge dislocation core energies than screw dislocation core energies. This can be understood because the swelling of hydrogen atoms can mitigate the tensile strains at the edge dislocation core whereas screw dislocations do not create tensile strains.
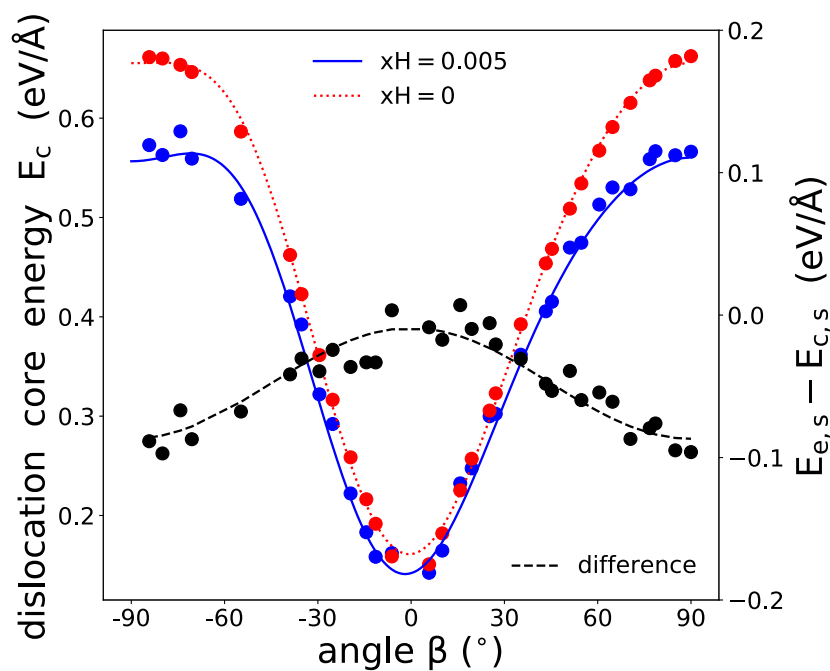
Figure 3. Dislocation core energy E_c as a function of dislocation character angle β for systems without and with 0.005 hydrogen. The hydrogen-induced difference in edge ($E_{c,e}$) and screw ($E_{c,s}$) core energies shows a $\cos^2$-like relationship with character angle.

Previous theoretical work [20] found that the difference in Gibbs energy of the core upon loading with hydrogen, $\frac{\Delta G_c}{\mu b^2}$, also changes with character angle. For similar loading conditions they find $\frac{\Delta G_{c,edge} - \Delta G_{c,screw}}{\mu b^2} \sim$ -0.02 when H-H interactions are ignored. Taking $\Delta E_c = E_c$ ($x_H = 0.005$) - E_c ($x_H = 0$) as an approximation for ΔG_c, we fit our MD data to a $\cos^2$ function. We see a good fit (Fig. 5 black dashed line), with $\frac{\Delta E_{c,edge} - \Delta E_{c,screw}}{\mu b^2} \sim -0.05$ for our systems. H-H interactions will lower the value of $\frac{\Delta G_c}{\mu b^2}$ so our result is reasonable in comparison to previous theoretical work.

Fig. 4 compares our MD dislocation energies with isotropic theory predictions using a parity plot. Both hydrogen-free and hydrogen-containing systems match well to the line. This shows that the isotropic expression is sufficient to describe the MD dislocation energies obtained from our α-Fe systems, otherwise we'd expect larger errors. It provides a strong foundation for DDD methods which usually assume an isotropic approximation.
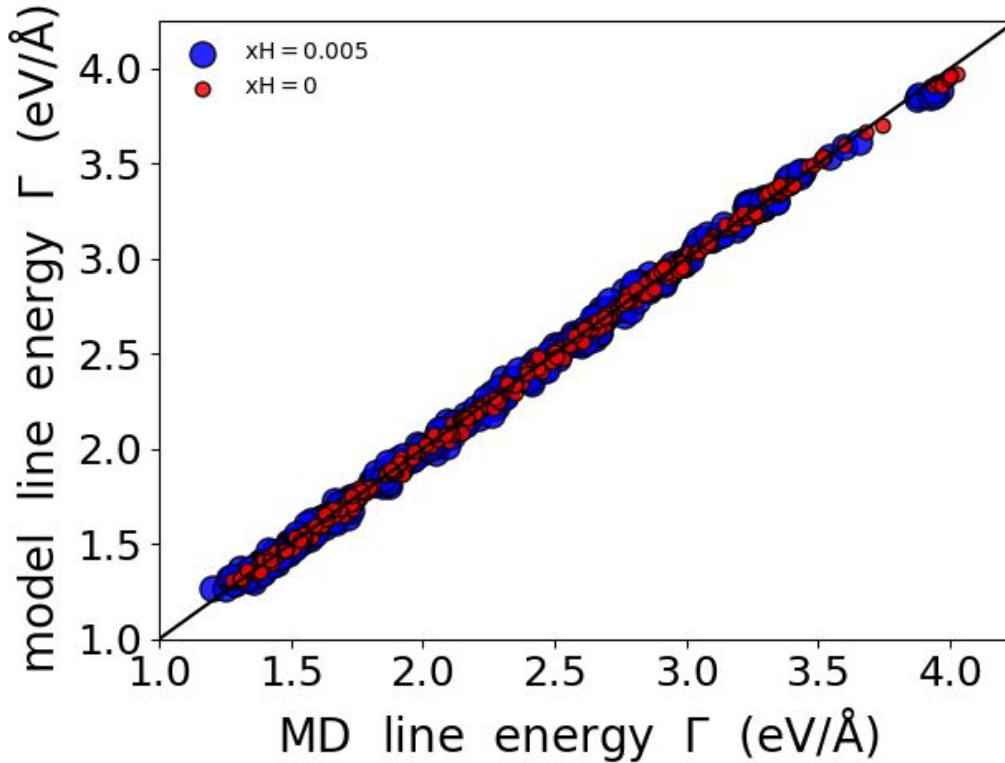
Figure 4. Parity plot between dislocation energies obtained from MD and isotropic theory for both hydrogen-free and hydrogen-containing systems.

C. *Dislocation Interaction Energies*

The screening of dislocation stress fields by hydrogen is one key aspect of the proposed HELP mechanism [4-6]. The screening would mean a reduction of dislocation interaction energies. Dislocation interaction energy is defined as the relative energy of interacting dislocations with respect to a reference energy where dislocations are far separated, i.e., $E_{int} = \Gamma - \Gamma_{ref}$ where Γ_{ref} is the dislocation line energy calculated from Eq. (7) using a chosen reference state. As pointed out above, infinitely separated dislocations have infinite energies. However, if dislocations have infinite separation distance S but finite separation distance $d = L_y/2$, dislocation energies converge to Eq. (6). As a result, we use the dislocation energies at $d = L_y/2 = 1000$ Å and $S = \infty$ as our reference state. In Fig. 5 we plot the interaction energy between the dislocation dipole for $d = L_y/2$

~ 98 Å and S ~80 Å across character angle, with and without hydrogen. Interestingly, interaction energies at x_H = 0.0, and 0.005 are similar, suggesting minor hydrogen effects as opposed to a simple screening effect. In fact, the interaction energy only appears to slightly decrease for edge-like dislocations (β ~ ±90°) and slightly increase for screw-like dislocations (β ~ 0°). This is consistent with the fitted shear moduli and Poisson's ratios. The interaction energy of screw dislocations is proportional to shear modulus G and hydrogen reduces G from 0.774 eV/Å³ to 0.749 eV/Å³ so that the 0.005 hydrogen should reduce the interaction energy by ~1%. The interaction energy of edge dislocations is proportional to G/(1-ν) and hydrogen increases G/(1-ν) from 1.319 eV/Å³ to 1.323 eV/Å³ so that the 0.005 hydrogen should increase the interaction energy by ~1%. While the character angle dependent hydrogen effects on dislocation interaction energy may be specific to the anisotropic system we explored, the minor hydrogen screening effect may be general and should be considered when interpreting the HELP mechanism in future studies.
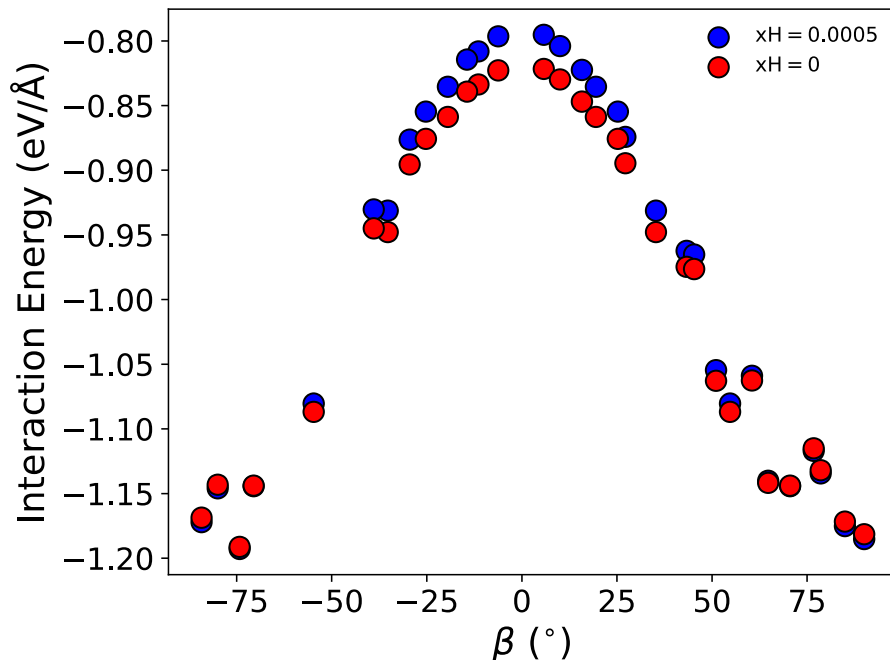
Figure 5. Dislocation interaction energy as a function of character angle β for systems with and without 0.005 hydrogen. Values are obtained at $d = L_y/2 \sim 98$ Å and $S \sim 80$ Å with respect to a reference of $d = L_y/2 \sim 1000$ Å and $S = \infty$.

IV.   DISCUSSIONS

Deformation in BCC metals is often limited by screw dislocation mobility because these dislocations can have non-planar core structures and are therefore less mobile than edge dislocations [34]. Thus, understanding how hydrogen interacts differently with screw and edge dislocations is important. Our work provides an opportunity to address this by examining the hydrogen population around both types of dislocations. Because we could not study $\beta = 0^o$, we compare results between a near-screw ($\beta = 5.77^o$) case with an edge case ($\beta = 90^o$). Based on the time-averaged MD approach [21,22], we calculated the hydrogen concentration field around the two types of dislocations, and the results are shown in Figs. 6(a) and 6(b) for $\beta = 5.77^o$ and $\beta = 90^o$, respectively. The plotted concentrations are normalized such that the average across all voxels is 1. Several observations can be made: (1) Hydrogen concentration is elevated at dislocations cores, forming hydrogen Cottrell atmosphere. This occurs not only in edge dislocations, but also in the near-screw dislocations despite that screw dislocations do not have tensile strain field which is the main driving force for hydrogen segregation; (2) the peak hydrogen concentration at dislocation cores is higher in the edge dislocation case than the near-screw case, consistent with the tensile strain of the edge dislocation; (3) the size of the H-segregated zone is smaller in the near-screw case than in the edge case, and the increased size in the edge case occurs exclusively in the x direction (i.e., on the slip plane); and (4) while hydrogen seems to be everywhere in the near-screw case, hydrogen mostly lies between 48 Å < y < 146 Å in the edge case (i.e., tensile

region). These features should be considered when explaining hydrogen effects on screw and edge dislocation migration.
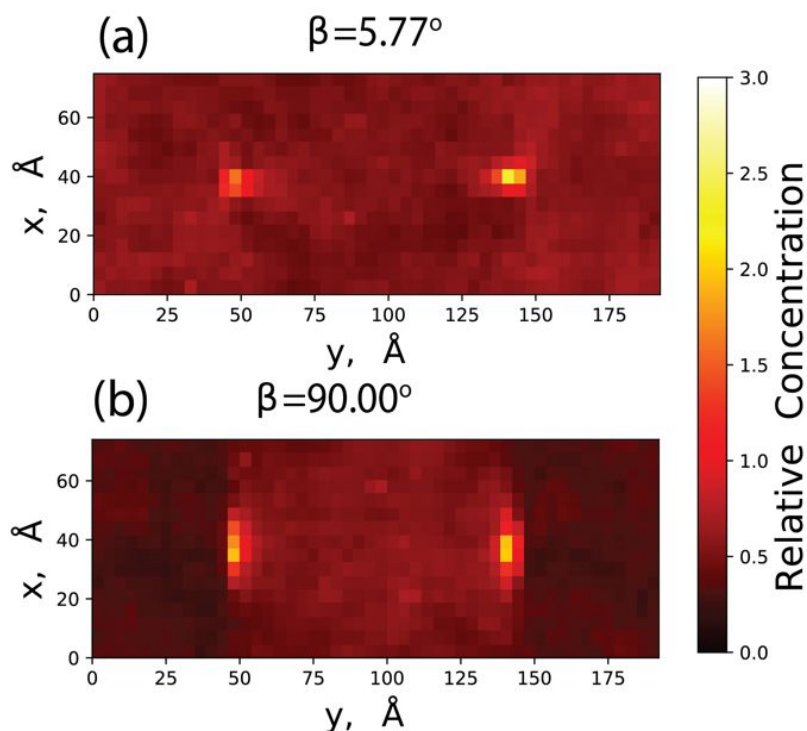

Figure 6. Concentration maps of H for (a) near-screw ($\beta = 5.77°$) and (b) edge ($\beta = 90.00°$) systems.

Our results show that hydrogen reduces dislocation core energies. Interestingly, hydrogen causes more significant core energy reduction when dislocation character angle approaches edge value (90°). Conventionally, the migration of screw dislocations in BCC metals is believed to proceed through a kink-pair mechanism [35]. The significant reduction of core energy of edge dislocations is hypothesized to give a lower barrier to form kink-pairs and therefore a higher kink-pair density, suggesting that hydrogen will increase screw dislocation mobility. However, care should be taken because hydrogen also imposes a drag force on the dislocation migration [36,37]. This interplay between kink-pair density and dislocation drag was investigated by Katzarov, et. al. using a kinetic Monte Carlo model [10]. They found that depending on the model parameters, the

dislocation velocity can increase by 3 orders of magnitude or decrease by an order of magnitude. One significance of our work is that we can provide calculated parameters rather than assumptions. We found that 0.005 hydrogen would cause about -0.078 eV/Å more core energy reduction for edge dislocation than screw dislocation, which can be used to estimate the kink-pair nucleation barrier required by their model. We also note that their model assumes that hydrogen atoms are "in front" of the moving dislocation. Our simulations do not require this assumption. Direct studies of hydrogen effects on screw dislocation mobility are beyond the scope of the present work but will be explored in the future.

V.   CONCLUSIONS

Molecular dynamics simulations performed in this work have resulted in the following conclusions:

1. The time-averaged approach can be used to compute hydrogen effects on dislocation energies in body-centered-cubic metals as a function of dislocation character angle. This success opens new opportunities to study hydrogen effects in BCC metals [38-40].

2. The isotropic elasticity theory can satisfactorily describe dislocation energy as a function of dislocation character angle even for anisotropic systems.

3. Hydrogen reduces dislocation core energies and modulates dislocation elastic energies in the entire dislocation character angle range -90° – 90°. However, the energy reduction is more significant for near edge dislocations than for near-screw dislocations. This means that hydrogen may promote mobility of screw dislocations via kink-pair nucleation.

4. The hydrogen-induced modification of dislocation interaction energy is minor, raising questions about the hydrogen screening mechanism of HELP [5,6].

5. The hydrogen Cottrell atmosphere around edge-like dislocations show greater enrichment in hydrogen concentration as compared to screw-like dislocations.

VI. ACKNOWLEDGEMENTS

VII. REFERENCES

1. Pfeil, L. B. The effect of occluded hydrogen on the tensile strength of iron. *Proc. Roy. Soc. A* **1926**, 112, 182-195.
2. Escober, D. P.; Depover, T.; Wallaert, E.; Duprez, L.; Verhaege, M.; Verbeken, K. Thermal desorption spectroscopy study of the interaction between hydrogen and different microstructural constituents in lab case Fe-C alloys. *Corr. Sci.* **2012**, 65, 199-208.
3. Cottrell, A. H.; Bilby, B. A. Dislocation theory of yielding and strain ageing of iron. *Proc. Phys. Soc. A* 1949, 62(1), 49.
4. Robertson, I. M.; Sofronis, P.; Nagao, A.; Martin, M. L.; Wang, S.; Gross, D. W.; Nygren, K. E. Hydrogen embrittlement understood. *Metall. Mater. Trans. B* **2015**, 46, 2323-2341.
5. Birnbaum, H. K.; Sofronis, P. Hydrogen-enhanced localized plasticity—a mechanism for hydrogen-related fracture. *Mater. Sci. Eng. A* **1994**, 176(1-2), 191-202.
6. Sofronis, P.; Birnbaum, H. K. Mechanics of the hydrogen-dislocationd-impurity interactions—I. Increasing shear modulus. *J. Mech. Phys. Solids* **1994**, 43(1), 49-90.
7. Stroh, A. N. A theory of the fracture of metals. *Adv. Phys.* **1957**, 6(24), 418-465.
8. Bhatia, M. A.; Groh, S.; Solanki, K. N. Atomic-scale investigation of point defects and hydrogen-solute atmospheres on the edge dislocation mobility in alpha iron. J. Appl. Phys. 2014, 116, 064302.
9. Itakura, M.; Kaburaki, H.; Yamaguchi, M.; Okita, T. The effect of hydrogen atoms on the screw dislocation mobility in bcc iron: a first-principles study. *Acta Mater.* **2013**, 61, 6857-6867.
10. Katzarov, I. H.; Pashov, D. L.; Paxton, A. T. Hydrogen embrittlement I. Analysis of hydrogen-enhanced localized plasticity: Effect of hydrogen on the velocity of screw dislocations in α-Fe. *Phys. Rev. Mater.* **2017**, 1, 033602.
11. Sills, R. B.; Cai, W. Free energy change of a dislocation due to a Cottrell atmosphere. *Phil. Mag.* **2018**, 98(16), 1491-1510.

12. Yu, P.; Cui, Y.; Zhu, G. Z.; Shen, Y.; Wen, M. The key role played by dislocation core radius and energy in hydrogen interaction with dislocations. *Acta Mater.* **2020**, 185, 518-527.
13. Clouet, E.; Ventelon, L.; Willaime, F. Dislocation core energies and core fields from first principles. PRL **2009**, 102(5), 055502.
14. Hirth, J. P. On dislocation interactions in the fcc lattice. *J. Appl. Phys.* **1961**, 32(4), 700-706.
15. Cotterill, R. M. J.; Doyama, M. Energy and atomic configuration of complete and dissociated dislocations. I. Edge dislocation in an fcc metal. *Phys. Rev.* **1966**, 145(2), 465.
16. Li, J.; Wang, C. Z.; Chang, J. P.; Cai, W.; Bulatov, V. V.; Ho, K. M.; Yip, S. Core energy and Peierls stress of a screw dislocation in bcc molybdenum: A periodic-cell tight-binding study. *Phys. Rev. B* **2004**, 70(10), 104113.
17. Yan, J. A.; Wang, C. Y.; Wang, S. Y. Generalized-stacking-fault energy and dislocation properties in bcc Fe: A first-principles study. *Phys. Rev. B* **2004**, 70(17), 174105.
18. Sills, R. B.; Kuykendall, W. P.; Aghaei, A.; Cai, W. Fundamentals of dislocation dynamics simulations. In Multiscale materials modeling for nanomechanics. In: Weinberger, C. R; Tucker, G. J., editors. Multiscale Materials Modeling for Nanomechanics, Springer Cham.; 2016, p. 53-87.
19. Deka, N.; Sills, R. B. Monte Carlo-Discrete Dislocation Dynamics: a technique for studying the formation and evolution of dislocation structures. *Model. Simul. Mat. Sci. Eng.* **2021**, 30(2), 024002.
20. Sills, R. B.; Bertin, N.; Aghaei, A.; Cai, W. Dislocation networks and the microstructural origin of strain hardening. *PRL* **2018**, 121(8), 085501.
21. Zhou, X. W.; Sills, R. B.; Ward, D. K.; Karnesky, R. A. Atomistic calculations of dislocation core energy in aluminium. *Phys. Rev. B* **2017**, 95(5), 054112.
22. Zhou, X. W.; Foster, M. E. Character angle effects on dissociated dislocation core energy in aluminum. *Phys. Chem. Chem. Phys.* **2021**, 23(5), 3290-3299.
23. Bertin, N.; Cai, W.; Aubry, S.; Bulatov, V. V. Core energies of dislocations in bcc metals. *Phys. Rev. Mater.* **2021**, 5(2), 025002.
24. Zhou, X.; Foster, M. E.; Ronevich, J. A.; San Marchi, C. W. Review and construction of interatomic potentials for molecular dynamics studies of hydrogen embrittlement in Fe─ C based steels. *J. Comp. Chem.* **2020**, 41(13), 1299-1309.
25. Kim, S. A.; Johnson, W. L. Elastic constants and internal friction of martensitic steel, ferritic-pearlitic steel, and α-iron. Materials Science and Engineering: A **2007**, 452, 633-639.
26. Souissi, M.; Numakura, H. Elastic properties of Fe–C and Fe–N martensites. ISIJ International, **2015**, 55(7), 1512-1521.
27. Thompson, A. P.; Aktulga, H. M.; Berger, R.; Bolintineanu, D. S.; Brown, W. M.; Crozier, P. S.; in't Veld, P. J.; Kohlmeyer, A.; Moore, S. G.; Nguyen, T. D.; Shan, R.; Stevens, M. J.; Tranchida, J.; Trott, C.; Plimpton, S. J. LAMMPS-a flexible simulation tool for particle-based materials modeling at the atomic, meso, and continuum scales. *Comput. Phys. Commun.* **2022**, 271, 108171.
28. Plimpton, S. Fast parallel algorithms for short-range molecular dynamics. *J. Comp. Phys.* **1995**, 117, 1–19.
29. Nowak, C.; Spataru, C. D.; Chu, K.; Zhou, X. W.; Sills, R. B. Molecular Dynamics Study of Hydrogen Cottrell Atmosphere in Aluminum: Influence of Solute-Solute Interactions in the Dislocation Core **2022** *submitted for review*
30. Nowak, C.; Foster, M. E.; Sills, R. B.; Zhou, X. W. Modulating Hydrogen Cottrell Atmosphere around Dislocations through Alloy Design of Austenitic Stainless Steels **2022** *to be submitted*
31. Cai, W.; Bulatov, V. V.; Chang, J.; Li, J.; Yip, S. Anisotropic elastic interactions of a periodic dislocation array. *PRL* **2001**, 86(25), 5727.
32. Cai, W.; Bulatov, V. V.; Chang, J.; Li, J.; Yip, S. Periodic image effects in dislocation modelling. *Phil. Mag.* **2003**, 83(5), 539-567.

33. Zhou, X. W.; Ward, D. K.; Zimmerman, J. A.; Cruz-Campa, J. L.; Zubia, D.; Martin, J. E.; van Swol, F. An atomistically validated continuum model for strain relaxation and misfit dislocation formation. *J. Mech. Phys. Solids* **2016**, 91, 265-277.

34. Lu, Y.; Zhang, Y. H.; Ma, E.; Han, W. Z. Relative mobility of screw versus edge dislocations controls the ductile-to-brittle transition in metals. *PNAS*, 2021 118(37)

35. Gordon, P. A.; Neeraj, T.; Li, Y.; Li, J. Screw dislocation mobility in BCC metals: the role of the compact core on double-kink nucleation. *Model. Simul. Mat. Sci. Eng.* **2010**, 18(8), 085008.

36. Sills, R. B.; Cai, W. Solute drag on perfect and extended dislocations. *Phil. Mag.* **2016**, 96(10), 895-921.

37. Epperly, E. N.; Sills, R. B. Transient solute drag and strain aging of dislocations. *Acta Mater.* **2020**, 193, 182-190.

38. Davies, R. G. Influence of martensite content on the hydrogen embrittlement of dual-phase steels. *Scripta Met.* **1983**, 17, 889-892

39. Ronevich, J.; Speer, J.; Matlock, D. Hydrogen embrittlement of commercially produced advanced high strength sheet steels. *SAE Int. J. Mater. Manuf.* **2010**, 3, 255-267.

40. Ronevich, J. A; De Cooman, B. C.; Speer, J. G.; De Moor, E.; Matlock, D. K. Hydrogen effects in prestrained transformation induced plasticity steel. *Met. Mater. Trans. A* **2012**, 43A, 2293-2301.